

The Kondo state in quantum point contacts and the local moment in semiconductor quantum dots - two sides of the same phenomenon.

Daniel L. Miller
Intel Electronics, P.O.Box 3173
Jerusalem 91031, Israel
Daniel.Miller@Intel.Com
 (November 23, 2018)

This is a three step work: i) we explain why quantum point contacts are similar to ballistic quantum dots; ii) we introduce the virtual Kondo state in both systems; iii-1st) this state explains 0.7 structure in point contacts; iii-2nd) formation of the local moment on this state is described by the nearly symmetric Anderson model, we solve it for finite size system having in mind quantum dots. We found one large level spacing $\Delta^* \propto (U\Gamma)^{1/2} \gg \Delta$, where U is the charging energy of the virtual state, Γ is the spectral width of this state and Δ is the mean level spacing of whole system. The theory explains periodicity of abnormal level spacing vs gate potential. The theory is in agreement with many experiments.

I. WHY QUANTUM POINT CONTACTS ARE SIMILAR TO CHAOTIC QUANTUM DOTS.

In this work we develop common view on two types of experiments, first, differential conductivity of quantum point contacts¹⁻³, and second, fluctuations of level spacing in semiconductor quantum dots^{4-8,7}. The challenge in the former case is to understand the plateau of differential conductance $dI/dV \approx 0.7(2e^2/h)$, which indicates presence of the Kondo state³. The Kondo state can appear from a magnetic impurity, as in the case of metallic point contacts¹⁰, however the point contact was made by electrodes on top of clean 2d electron gas¹⁻³.

The level spacing fluctuation in the latter case indicates presence of a local moment inside the dot¹¹. There are two possibilities: either magnetic moment is formed on the localized Kondo state or the magnetic moment is formed due to the Stoner instability of electron system^{12-14,7}. However, the clean semiconductor quantum dots do not have magnetic impurities and formation of the Kondo state is unrealistic. The Stoner instability occurs under very restrictive condition met only in some experiments^{16,17}.

The anticipated Kondo state can be found in both systems, quantum point contact and semiconductor quantum dot, as a virtual state bouncing along shortest axis of the system. This state is marked by dashed line in Fig. 1a for contact geometry and in Fig. 1b for real potential of rectangular quantum dot^{18,19}. We assume that the system is ballistic, $l \gtrsim l_p$, where l is the mean free path and l_p is the length of the virtual state. This state is very unstable indeed, the electron lifetime on such orbit \hbar/Γ is of the order of the time of flight l_p/v_F , in other words level uncertainty of such state is of the order of level spacing $\Gamma \sim \pi\hbar^2 k_F/ml_p$,

where k_F is the Fermi momentum and m is the effective mass. This state is important for two main reasons i) it has good coupling to all other “chaotic” wave functions^{20,21} ii) it cost extra energy to put two electrons on this state compare to all other “chaotic” wave

functions spread across whole system; the enhancement factor is approximately $\log(k_F l_p)$.

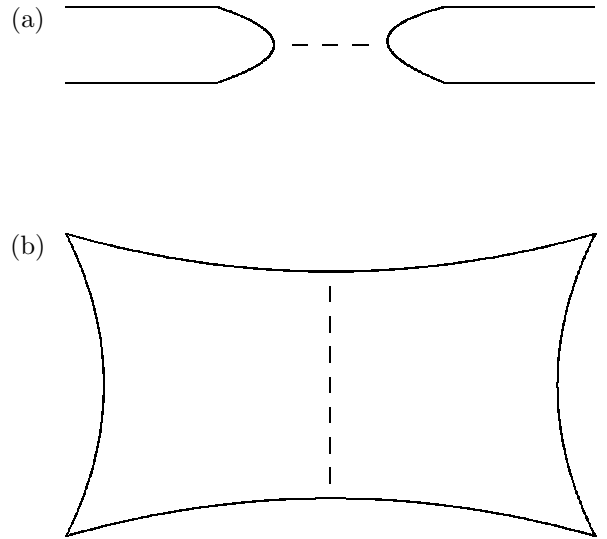


FIG. 1. Local moment (Kondo state) is formed on unstable periodic trajectory between tips of quantum point contact (a) or across quantum dot (b). This orbit traps electrons for some time and have high charging energy.

The sweep of the gate potential in both dots and contacts raise the Fermi level; the singly occupied Kondo state floats on the Fermi level^{22,23}. In this way conductance of the point contact at zero bias is given by resonant conductance of Kondo state. The level spacing of the quantum dot is almost the same as of a non-interacting system. When the Fermi level reaches “symmetric” limit position, the virtual state can be doubly occupied. The system becomes effectively non-interacting. At this gate potential one observes kink of the level spacing in the

quantum dot. In other words, the thermodynamic limit of the symmetric Anderson model is incompressible electron liquid, and finite size system has just pseudogap.

In the next section we derive effective Hamiltonian by making use of Green function technique and arrive at the Anderson model. The nearly symmetric limit is better to explore by making use of the Wiegmann solution, that is done in Section III. We solve Bethe equation with one energy level split out of the band, the “gap” energy is exactly the experimentally observed kink in the level spacing. Section IV provides analysis of some experimental data and summary.

II. HAMILTONIAN OF THE VIRTUAL STATE.

Single electron wave functions $\psi_j(\vec{r})$ of a classically chaotic system are inhomogeneous. Consider an unstable periodic orbit p in a system with two degrees of freedom. Such an orbit contributes to the density of states at the energy ϵ the sum²⁴

$$\frac{-T_p}{2\pi\hbar} \text{Im} \sum_{m=1}^{\infty} \frac{1}{\sinh(\Lambda_p m/2)} e^{imS_p(\epsilon+i0)/\hbar}, \quad (1)$$

where $T_p = \partial S_p / \partial \epsilon$ is the period of the orbit, $S_p(\epsilon)$ is the action of the orbit, $S_p(\epsilon)$ includes the phase changes at the conjugated points, $\Lambda_p > 0$ is the stability exponent.

Let us assume that p is the only one relatively stable $\Lambda_p \lesssim 1$ periodic orbit in the system. In this particular case p contributes a sequence of Lorentzians²⁴ to the density of states:

$$\sum_n T_p(\epsilon) \frac{\Lambda_p \hbar}{[S_p(\epsilon) - 2\pi n \hbar]^2 + (\Lambda_p \hbar/2)^2}. \quad (2)$$

Each term in the sum can be regarded as the spectral function of the “scar” state

$$A_n(\epsilon) = \frac{1}{\pi} \frac{\Gamma_n}{(\epsilon - \epsilon_n)^2 + \Gamma_n^2}, \quad (3)$$

where $\Gamma_n = \Lambda_p \hbar / (2T_p(\epsilon_n))$.

This spectral function tell us that it is possible to construct a non-stationary solution $\psi_n(r)$ to the Schroedinger equation in the vicinity of orbit p . This solution, let us call it “scar”²⁵, would decay to “flat” states with the rate Γ_n/\hbar . The matrix elements of the decay process V_{jn} are not known, but it is clear that

$$\Gamma_n = \pi \sum_j |V_{jn}|^2 A_n(\epsilon_j), \quad (4)$$

where ϵ_j are energies of the exact wave functions. Fortunately we will not need explicit values of V_{jn} in further calculations.

In what follows let us assume that electrons fill the system up to the Fermi energy at zero temperature. Let $n = d$ is the first “scar” state below the Fermi energy E_F . The Hamiltonian for states in the vicinity of the Fermi level is

$$\hat{\mathcal{H}} = \sum_{\sigma} \left\{ \sum_{\substack{\epsilon_j < D_{d+1} \\ j, \epsilon_j > D_d}} [\epsilon_j a_{j\sigma}^{\dagger} a_{j\sigma} + V_{jd} a_{j\sigma}^{\dagger} a_{d\sigma} + \text{h.c.}] + \epsilon_d a_{d\sigma}^{\dagger} a_{d\sigma} \right\}, \quad (5)$$

$$D_d = (\epsilon_d + \epsilon_{d-1})/2, \quad (6)$$

and formulation of the Anderson impurity model²⁶ is accomplished by adding the correlation energy

$$\hat{\mathcal{H}}_{\text{corr}} = U \hat{n}_{d\uparrow} \hat{n}_{d\downarrow}, \quad (7)$$

with

$$U = \int d\vec{r}_1 d\vec{r}_2 |\psi_d(\vec{r}_1)|^2 |\psi_d(\vec{r}_2)|^2 \frac{e^2}{|\vec{r}_1 - \vec{r}_2|}. \quad (8)$$

It should be much larger than the charging energy of the dot, U_j , given in general by

$$U_j = \int d\vec{r}_1 d\vec{r}_2 |\psi_j(\vec{r}_1)|^2 |\psi_j(\vec{r}_2)|^2 \frac{e^2}{|\vec{r}_1 - \vec{r}_2|}. \quad (9)$$

and almost the same for all flat states ψ_j .

The contribution of p to the Green function of the non-interacting system has the form $G(r, r) \propto e^{iW(x)y^2/\hbar}$, where $\vec{r} = (x, y)$, x is the coordinate along the orbit p , the y axis is perpendicular to the orbit p at the point x , and $W(x)$ is connected with the second derivatives of the action. Then, the width of the “scar” state is estimated as $\sim \sqrt{\hbar/W}$. It is clear that $W(x) \sim k/l_p$, where $k = \sqrt{2m\epsilon_d/\hbar}$, and m is the mass of the particle, see for example the analysis of chaotic billiards²⁷. The integral Eq. (9) for the wave function concentrated in the rectangle of the width $\sim \sqrt{l_p/k}$ and length l_p gives $U \sim \frac{e^2}{l_p} (\log \sqrt{kl_p} - 1)$. For experiment of Sivan *et al*⁴ $kl_p \sim 100$ and the correlation energy U is large.

To summarize the section both a quantum dot and a point contact can have virtual quasi one-dimensional state at the energy ϵ_d ; the charging energy of the state is U . This state is well coupled to a finite number of “flat” chaotic states in certain energy interval. So we have all ingredients of the Anderson impurity model. It allows to compute valence of the impurity state and other thermodynamic properties. Our primary interest is the compressibility of the electron system at formation/disappearance of magnetic moment. This regime is described by the almost symmetric limit of the model, see the next section.

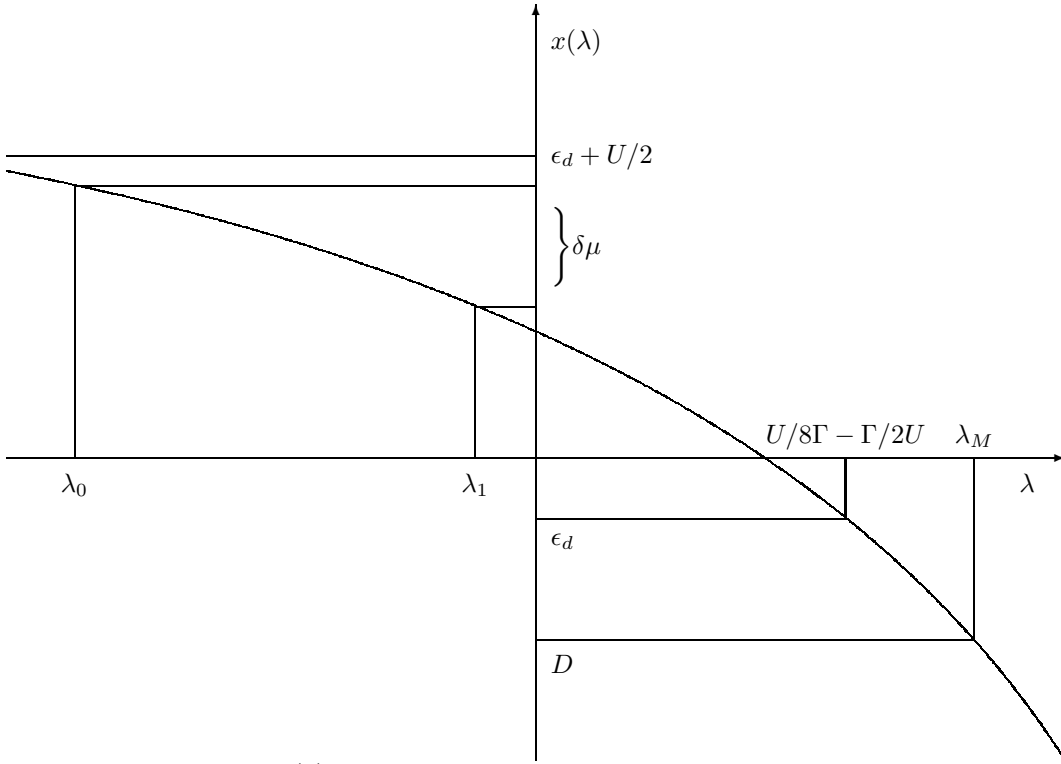


FIG. 2. The function $x(\lambda)$ as it appears in Bethe equations, Eq. 36. The rapidities λ_α lie in the interval $[\lambda_0, \lambda_M]$, corresponding energies lie between band bottom D and chemical potential $\mu \approx x(\lambda_0)$. In the symmetric limit $\mu \sim \epsilon_d + U/2$ and in the assymmetric limit $\mu \sim \epsilon_d$, where ϵ_d is the energy of the virtual state, and U is the charging energy.

III. THE LEVEL SPACING IN PRESENCE OF THE KONDO STATE.

The purpose of this section is to compute the ground state energy E_N of N -particle chaotic system in presence of the Kondo interaction with quasi-one-dimensional state. Then we will compute the chemical potential $\mu_N = E_{N+1} - E_N$ and the inverse compressibility (the level spacing) of whole system $\Delta_* = \mu_N - \mu_{N-1}$. This quantity is interesting in vicinity of the symmetric regime, when spin is just disappears and we expect strong fluctuations.

Wiegmann have solved this problem in one dimension²⁸. However dimensionality of the system is not important since j -states do not interact with themselves. In order to apply the Wiegmann solution we need to postulate the constant energy spacing 2Δ between j -states. This approximation is not bad in chaotic systems due to level repulsion.

At the zero magnetic field the ground state is described by the set of rapidities $\{\lambda_\alpha\}_{\alpha=0}^M$, where $M+1$ is number of down spins. The rapidities satisfy

$$J_\alpha + \frac{1}{\pi} \sum_{\beta=0}^M \arctan(\lambda_\alpha - \lambda_\beta) = -\frac{1}{\Delta} [x(\lambda_\alpha) + O(\Delta)] \quad (10)$$

$$x(\lambda) = \epsilon_d + U/2 - (U\Gamma)^{1/2} (\lambda + (\lambda^2 + 1/4)^{1/2})^{1/2}, \quad (11)$$

$\Gamma = |V|^2$ is also constant. We keep here terms in the lowest order in Δ . The integer numbers $\{J_\alpha\}_{\alpha=0}^M$ completely

describe the state of the system with $N = 2(M+1)$ particles. The energy of the system is just

$$E = 2 \sum_{\alpha=0}^M x(\lambda_\alpha). \quad (12)$$

The ground state corresponds to subsequent values of J_α , fixed by the condition

$$J_\alpha < J_M, \quad \lambda_\alpha < \lambda_M, \quad x(\lambda_\alpha) > x(\lambda_M) = D \quad (13)$$

where D is the bottom of the energy band, see Fig. 2.

The ground state is a bit more complicated for odd number of particles, $N = 2M + 1$. In this case $\alpha = 0 \dots M-1$, and we introduce new rapidity $\tilde{\lambda}$:

$$J_\alpha + \frac{1}{\pi} \sum_{\beta=0}^{M-1} \arctan(\lambda_\alpha - \lambda_\beta) + \frac{1}{\pi} \arctan(2\lambda_\alpha - 2\tilde{\lambda}) = -\frac{1}{\Delta} x(\lambda_\alpha) \quad (14)$$

$$\tilde{x}(\tilde{\lambda}) = \epsilon_d + U/2 - (2U\Gamma\tilde{\lambda})^{1/2} = D, \quad (15)$$

$$E = \tilde{x}(\tilde{\lambda}) + 2 \sum_{\alpha=0}^{M-1} x(\lambda_\alpha). \quad (16)$$

In order to compute the chemical potential we need both solutions Eq. (12) and Eq. (16), because one additional electron changes number of particles from odd to even or

vice versa. Fortunately, the difference between the odd-electron solution and the even-electron solution is small, something happens at the bottom of the band, and not near the Fermi surface. For this very reason we will define the chemical potential as half of energy one needs to add two particles to a system with even number of particles:

$$\mu_N \equiv \frac{E_{N+2} - E_N}{2}, \quad \Delta_* = \frac{\mu_N - \mu_{N-2}}{2}. \quad (17)$$

Here Δ_* is the level spacing of interacting system.

When the level spacing of non-interacting system is small $\Delta \rightarrow 0$, one can solve Eq. (10) by making use of the continuous approximation. It is justified by the condition

$$|\lambda_{\alpha+1} - \lambda_\alpha| \ll 1 \quad \forall \alpha. \quad (18)$$

So we replace sum Eq. (10) by integral

$$J_\alpha + \frac{1}{\Delta} \int_{\lambda_0}^{\lambda_M} \arctan(\lambda_\alpha - \lambda') \sigma(\lambda') d\lambda' = -\frac{1}{\Delta} x(\lambda_\alpha), \quad (19)$$

where $\sigma(\lambda) \sim \frac{\Delta/\pi}{\lambda_{\alpha+1} - \lambda_\alpha}$. Taking derivative with respect to λ_α we arrive at the integral equation

$$\sigma_\lambda + \frac{1}{\pi} \int_{\lambda_0}^{\lambda_M} \frac{\sigma_{\lambda'} d\lambda'}{1 + (\lambda - \lambda')^2} = -\frac{1}{\pi} \frac{dx}{d\lambda} \quad (20)$$

which can be formally solved in whole range $\lambda \in] -\infty, \lambda_M]$. For large λ_M we can write equation with $\alpha = M$ as $J_M + M/2 \approx -D/\Delta$, then all J_α s become fixed $J_\alpha = -D/\Delta - 3M/2 + \alpha$. Integrating Eq. (20) from $-\infty$ to λ_α (again λ_M is large) we get equation for λ_α :

$$\pi \int_{-\infty}^{\lambda_\alpha} \tilde{\sigma}_\lambda d\lambda = \epsilon_d + U/2 - D - 2M\Delta + \alpha\Delta. \quad (21)$$

where we made use of $x(-\infty) = \epsilon_d + U/2$.

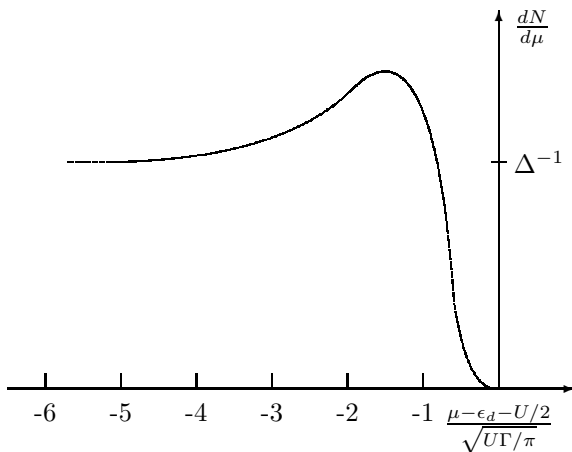


FIG. 3. The compressibility of electron gas in presence of the Anderson impurity. Electron system becomes incompressible in the mixed-valence regime.

The general (Wiener-Hopf) solution of Eq. (20) is available in the Wiegmann paper²⁹. The particular case $\lambda_0 = -\infty$ and $\lambda_M = \infty$ can be solved by Fourier transform method and the result is

$$\sigma_\lambda = \int_{-\infty}^{\infty} \frac{dk}{2\pi} \frac{1}{\cosh(\pi\lambda - \pi k^2/(2U\Gamma))} \quad (22)$$

it changes a little when λ_0, λ_M are finite but large. For large negative λ the solution behaves exponentially

$$\sigma_\lambda \approx \int_{-\infty}^{\infty} \frac{dk}{2\pi} 2e^{\pi\lambda - \pi k^2/(2U\Gamma)} = \sqrt{2U\Gamma} e^{\pi\lambda} \quad (23)$$

Then we can compute the lowest rapidity λ_0 from Eq. (21)

$$\lambda_0 = \frac{1}{\pi} \log \frac{\epsilon_d + U/2 - D - 2M\Delta}{\sqrt{2U\Gamma}} \quad (24)$$

and indeed it goes to $-\infty$ in the symmetric limit of the Anderson model

$\epsilon_d + U/2 - D - 2M\Delta \rightarrow 0$, (it is enough to have $|\epsilon_d + U/2 + D - 2M\Delta| \ll \sqrt{U\Gamma}$).

Solution Eq. (22) works for any λ_0 if $\lambda < \lambda_0$. Then we combine Eq. (22) with Eq. (36) and obtain compressibility

$$\frac{dN}{d\mu} = \frac{1}{\Delta} \int_{-\infty}^{\infty} \frac{dk}{2\pi} \frac{-\tilde{\mu} - \pi^2/4\tilde{\mu}^3}{\cosh((\pi^2/4 - \tilde{\mu}^4)/2\tilde{\mu}^2 - k^2/2)} \quad (25)$$

where $\tilde{\mu} = (\mu - \epsilon_d - U/2)/\sqrt{U\Gamma/\pi}$. The compressibility is zero at symmetric limit, see Fig. 3.

In the vicinity of symmetric limit one has simple expressions for chemical potential and level spacing

$$\begin{aligned} \mu_N &= x(\lambda_0) \\ &= \epsilon_d + U/2 - \sqrt{\frac{\pi U\Gamma/8}{\log(\sqrt{2U\Gamma}/A_N)}}, \\ \Delta_* &= \frac{\partial \mu}{\partial N} = \frac{\Delta}{A_N} \sqrt{\frac{\pi U\Gamma/32}{\log^3(\sqrt{2U\Gamma}/A_N)}}, \end{aligned} \quad (26)$$

$$A_N = \epsilon_d + U/2 - D - (N - 2)\Delta. \quad (27)$$

The level spacing Δ_* diverges for any fixed Δ in the vicinity of the symmetric limit. This result indicates that system is unstable near $\mu = \epsilon_d + U/2$, and experimentally one observes kinks of level spacing.

The kink of the level spacing means that the system becomes non-interacting, the chemical potential gets its $U = 0$ value

$$\mu_N|_{U=0} = N\Delta + D, \quad (28)$$

and the observed kink is

$$\begin{aligned}\Delta_* &= \mu_N|_{U=0} - \mu_{N-2}, \\ &= \sqrt{\frac{\pi U \Gamma / 8}{\log(\sqrt{2U\Gamma}/A_{N-2})}} - A_N.\end{aligned}\quad (29)$$

The maximal possible kink of the level spacing is

$$\Delta_{\max} = \sqrt{\frac{\pi U \Gamma / 4}{\log(U\Gamma/2\Delta)}} \gg \Delta. \quad (30)$$

It goes to zero in thermodynamic limit $\Delta \rightarrow 0$, but remains large. We will derive Eqs. (30,eq:model.res2) in the rest of the section.

The problem is that the condition Eq. (18) is broken for the lowest λ_α near the symmetric limit. Since for $\lambda_0 \rightarrow -\infty$ the density of the rapidities goes to zero exponentially, so $|\lambda_1 - \lambda_0| \propto e^{\pi|\lambda_0|\Delta/\sqrt{U\Gamma}}$ can be very large for any fixed Δ . The main idea of the present paper is to introduce one rapidity λ_0 separated from all the rest $\lambda_1 \dots \lambda_M$. We should assume $|\lambda_0 - \lambda_1| \gg 1$ in Eq. (19) with $\alpha = 0$:

$$J_0 - \frac{M}{2} - \frac{1}{\Delta} \int_{\lambda_1}^{\lambda_M} \frac{\sigma_\lambda d\lambda}{\lambda_0 - \lambda} = -\frac{1}{\Delta} (\epsilon_d + U/2 - \sqrt{\frac{U\Gamma}{8|\lambda_0|}}) \quad (31)$$

where we expanded $\arctan()$. The integral equation for region of "dense" rapidities becomes

$$\sigma_\lambda + \frac{\Delta/\pi}{1 + (\lambda - \lambda_0)^2} \frac{1}{\pi} \int_{\lambda_1}^{\lambda_M} \frac{\sigma_{\lambda'} d\lambda'}{1 + (\lambda - \lambda')^2} = -\frac{1}{\pi} \frac{dx}{d\lambda} \quad (32)$$

In the lowest order in $1/\lambda_0$ we neglect the integral in Eq. (31) and obtain $x(\lambda_0)/\Delta = M/2 - J_0 = 2M + D$ that is equivalent to Eq. (30). Lowest rapidities are

$$\lambda_0 \approx -U\Gamma/8A_N^2, \quad \lambda_1 = \frac{1}{\pi} \log\left(A_{N-2}/\sqrt{2U\Gamma}\right), \quad (33)$$

where λ_1 goes to $-\infty$ much slowly than λ_0 . Within the approximation made here λ_1 of system of $N + 2$ particles coincides with λ_0 of system of N particles. Then the obtained pseudogap Eq. (30) is just $x(\lambda_0) - x(\lambda_1)$.

In conclusion of the section we have found the anomalously large spacing between energy levels of electron gas interacting with impurity. This is a finite size effect, which requires special treatment. The pseudogap appears at the Fermi energy when the model approaches complete particle-hole symmetry, $\mu \approx \epsilon_d + U/2$.

IV. EXPERIMENTAL DATA AND CONCLUSIONS.

Let us consider experiment, where one fills the system by particles. The Fermi level goes up $\mu(N) \sim N\Delta + D$, where N is the number of particles inside the system,

and D is the band offset. At the value $N = N_d$ given by equation

$$\mu(N_d) = \epsilon_d + U/2 \quad (34)$$

we arrive at the symmetric Anderson model. Just below this value of N the Fermi energy makes a large jump given by Eq. (29). Later we will measure the Δ_* in terms of mean level spacing

$$\delta_* = \Delta_*/\Delta \approx \sqrt{(\pi/4)x/\log x}, \quad x = U\Gamma/2\Delta^2 \gg 1. \quad (35)$$

The Fermi energy will jump again near $N = N_{d+1}$. The distance between jumps is $N_{d+1} - N_d \approx (\epsilon_{d+1} - \epsilon_d)/\Delta$ is inverse proportional to the length of the orbit l_p

$$\delta N = N_{d+1} - N_d \approx \frac{2L}{l_p} \sqrt{2\pi N_{d+1}}. \quad (36)$$

This formula was derived for $\Delta = \pi\hbar^2/(mA)$, where L is size of the quantum dot, $A \approx L^2$ is its area and $\delta N \ll N_{d+1}$.

The experimental data from few references is summarized in Table I. The first block contains data taken from cited papers, then we provide estimation of k_F , Δ , Γ , U , δN , and δ_* . Last block in Table I contains δN and δ_* taken from charts of $E_{N+1} - E_N$ vs N reported in cited papers.

Typically $l_p \sim 2L$ and we will use $\delta N = \sqrt{2\pi N_{d+1}}$. The Coulomb energy of the virtual state is $U \approx E_C \log k_F l_p$ where E_C is the charging energy of the dot, and k_F is wave number on Fermi surface. The coupling Γ is of the order of level spacing of virtual state, at least it larger than level spacing of host system: $\Delta \lesssim \Gamma \lesssim \epsilon_{d+1} - \epsilon_d$. For this reason Table I contains two values for Γ - minimal and maximal estimates. Last computed value is δ_* , which eventually have minimal and maximal estimates derived from Eq. (36). We see that our theory works well for clean samples^{4,30,6} and it is not applicable for disordered quantum dots⁵. The virtual state is absent in perfectly rectangular quantum dot⁹ (without shape deformations) as well.

The conductance of a quantum point contact (QPC) with the Kondo state inside has been computed recently³¹ and the model explained all the experimental data. Existence of the Kondo state in a QPC is very plausible, and therefore we expect to see Kondo state inside quantum dots too. The present theory should not be confused with Kondo effect due to charging of entire dot³². However the interesting feature of both types of experiments (Kondo state on "scar" and Kondo state inside entire dot) is that the gate voltage allows to scan all regimes of Anderson model³³.

To summarize, inhomogeneities of chaotic wave functions can be gathered together into an additional state of small size. In this way one arrives at Anderson's impurity model with finite number of free electron states. At certain value of the chemical potential the model has

complete particle-hole symmetry. The chemical potential does not approach this value gradually, but rather irregularly. The energy scale of this effect is a new combination of the parameters of Anderson's model and the mean level spacing. This scenario is a possible explanation of the irregularities observed experimentally in quantum dots.

¹ B. J. Wees, H. Houten, C. W. J. Beenakker, J. G. Williamson, L. P. Kouwenhoven, D. Marel and C. T. Foxon, *Phys. Rev. Lett.* **60**, 848 (1988).
² K. J. Thomas, J. T. Nicholls, M. Y. Simmons, M. Pepper, D. R. Mace, and D. A. Ritchie, *Phys. Rev. Lett.* **77**, 135 (1996).
³ S. M. Cronenwett, H. J. Lynch, D. Goldhaber-Gordon, L. P. Kouwenhoven, C. M. Marcus, K. Hirose, N. S. Wingreen, V. Umansky, *Phys. Rev. Lett.* **88**, 226805 (2002), [cond-mat/0201577].
⁴ U. Sivan, R. Berkovits, Y. Aloni, O. Prus, A. Auerbach, and G. Ben-Yoseph, *Phys. Rev. Lett.* **77**, 1123 (1996).
⁵ N. B. Zhitenev, R. C. Ashoori, L. N. Pfeiffer and K. W. West, *Phys. Rev. Lett.* **79**, 2308 (1997).
⁶ S. R. Patel, S. M. Cronenwett, D. R. Stewart, A. G. Huibers, C. M. Marcus, C. I. Duruöz, J. S. Harris, Jr., K. Campman and A. C. Gossard, *Phys. Rev. Lett.* **80**, 4522 (1998).
⁷ S. R. Patel, D. R. Stewart, C. M. Marcus, M. Gökçedä, Y. Alhassid, and A. D. Stone C. I. Duruöz, J. S. Harris, Jr., *Phys. Rev. Lett.* **81**, 5900 (1998), [cond-mat/9808166].
⁸ F. Simmel, D. Abusch-Magder, D. A. Wharam, M. A. Kastner, and J.P.Kotthaus, *Phys. Rev. B* **59**, 10441 (1999), [cond-mat/9901274].
⁹ S. Lucher, T. Heinzl, K. Ensslin, W. Wegscheider, and M. Bichler, *Phys. Rev. Lett.* **86**, 2118 (2001).
¹⁰ D. C. Ralph and R. A. Buhrman, *Phys. Rev. Lett.* **72**, 3401 (1994).
¹¹ R. Berkovits, *Phys. Rev. Lett.* **81**, 2128 (1998).
¹² A. V. Andreev and A. Kamenev, *Phys. Rev. Lett.* **81**, 3199 (1998).
¹³ P. W. Brouwer, Y. Oreg, and B. I. Halperin, *Phys. Rev. B* **60**, 13977 (1999).
¹⁴ I. L. Kurland, I. L. Aleiner, and B. L. Altshuler, *Phys. Rev. B* **62**, 14886 (2000), [cond-mat/0004205].
¹⁵ H. U. Baranger, D. Ullmo, L. I. Glazman, *Phys. Rev. B*

61, 2425 (2000).
¹⁶ P. Jacquod and A. D. Stone, (2001), [cond-mat/0102100].
¹⁷ J. A. Folk, C. M. Marcus, R. Berkovits, I. L. Kurland, I. L. Aleiner, B. L. Altshuler, (2000), [cond-mat/0010441].
¹⁸ M. Stopa, (1997), [cond-mat/9709119].
¹⁹ M. Stopa, *Microelectronic Engineering* **47**, 119 (1999).
²⁰ M. V. Berry, *J. Phys. A* **10**, 2083 (1977).
²¹ E. J. Heller, *Phys. Rev. Lett.* **53**, 1515 (1984).
²² F. D. M. Haldane, *Phys. Rev. Lett.* **40**, 416 (1978).
²³ M. Stopa, *Phys. Rev. B* **54**, 13767 (1996).
²⁴ M. C. Gutzwiller, *J. Math. Phys.* **12**, 343 (1971).
²⁵ E. J. Heller and S. Tomsovic, *Phys. Today* **46**, 38 (July 1993).
²⁶ P. W. Anderson, *Phys. Rev.* **124**, 41 (1961).
²⁷ E. B. Bogomolny, *Physica D* **31**, 169 (1988).
²⁸ P. B. Wiegmann, *Phys. Lett. A* **80**, 163 (1980).
²⁹ P. B. Wiegmann, *J. Phys. C* **16**, 2281 (1983).
³⁰ F. Simmel, T. Heinzl and D. A. Wharam, *Europhys. Lett.* **38**, 123 (1997).
³¹ Y. Meir, K. Hirose and N. S. Wingreen, (2002), [cond-mat/0207044].
³² L. Kouwenhoven and L. Glazman, *Phys. World* 33 (2001), [cond-mat/0104100].
³³ D. Goldhaber-Gordon, J. Göres, M. A. Kastner, H. Shtrikman, D. Mahalu, and U. Meirav, *Phys. Rev. Lett.* **81**, 5225 (1998), [cond-mat/9807233].

TABLE I. Measured data / Intermediate calculations / Observed values of δN and δ_* . energies are given in meV, length are given in μm and wavenumbers in μm^{-1} .

Ref.	4	30	5	6 [‡]
N	100	250	100	340
A	0.15	0.07	0.13	0.17
L	0.5	0.3	1.2 [†]	0.9
E_C	0.6	2	1	0.59
k	65	150	83	110
Δ	0.02	0.05	0.04	0.02
U	2.0	8	4.6	3
Γ	0.02 - 0.5	0.05 - 2.0	0.04 - 1.0	0.02 - 1.0
δN	25	40	25	46
δ_*	3 - 10	4 - 16	3 - 7	3 - 13
δN	15	22	5	-
δ_*	10	6-8	2	6

† – circumference ‡ – the sample # 1